Computational Feasibility Study of a Torsional Wave Transducer for Tissue Stiffness Monitoring

Rafael Muñoz, Juan Melchor, Alicia Valera, Laura Peralta, Guillermo Rus

Abstract—A torsional piezoelectric ultrasonic transducer design is proposed to measure shear moduli in soft tissue with direct access availability, using shear wave elastography technique. The measurement of shear moduli of tissues is a challenging problem, mainly derived from a) the difficulty of isolating a pure shear wave, given the interference of multiple waves of different types (P, S, even guided) emitted by the transducers and reflected in geometric boundaries, and b) the highly attenuating nature of soft tissular materials. An immediate application, overcoming these drawbacks, is the measurement of changes in cervix stiffness to estimate the gestational age at delivery. The design has been optimized using a finite element model (FEM) and a semi-analytical estimator of the probability of detection (POD) to determine a suitable geometry, materials and generated waves. The technique is based on the time of flight measurement between emitter and receiver, to infer shear wave velocity. Current research is centered in prototype testing and validation. The geometric optimization of the transducer was able to annihilate the compressional wave emission, generating a quite pure shear torsional wave. Currently, mechanical and electromagnetic coupling between emitter and receiver signals are being the research focus. Conclusions: the design overcomes the main described problems. The almost pure shear torsional wave along with the short time of flight avoids the possibility of multiple wave interference. This short propagation distance reduce the effect of attenuation, and allow the emission of very low energies assuring a good biological security for human use.

Keywords—Cervix ripening, preterm birth, shear modulus, shear wave elastography, soft tissue, torsional wave.

I. INTRODUCTION

ALTOUGH ultrasonic tissue characterization for clinical diagnosis has mainly been undertaken with longitudinal waves [1], shear waves has also been reported, since there are evidences that shear dynamic viscoelastic properties able to characterize the tissue state [2]–[5].

Recently, torsional waves have been proposed for tissue shear modulus characterization [6]. Torsional waves propagate at shear wave velocity [7]–[9] and have been reported to be highly sensitive to elastic properties changes in quasifluids and soft tissues, like those caused by tumors [10], [11]. Shear stiffness is correlated to tissue micro-structure, which in turn is more affected by pathologies than the fluid phase.

This work proposes a torsional transducer for shear modulus characterization of tissues. The methodological approach applied on its conception, allowed the almost total removal of P-wave emissions, as a main feature, so that misinterpretations are avoided due to interferences and mode conversions.

Rafael Muñoz is with the NDE Lab, Department of Structural Mechanics, University of Granada, Granada, 18071 Spain (phone: +34 958216141; fax: +34 95829959; e-mail: rmb@ugr.es).

Juan Melchor, Alicia Valera, Laura Peralta, Guillermo Rus are with the NDE Lab, Department of Structural Mechanics, University of Granada, Granada, 18071 Spain (e-mail: jmelchor@ugr.es, avaleramartinez@gmail.com, lperalta@ugr.es, grus@ugr.es).

From the methodological point of view, the geometric parameters of the proposed transducer has been optimized with a maximization criterion of its probability of detection (POD) on shear modulus changes.

II. METHODS

A. Initial Conceptual Design of the Transducer

Figs. 1 and 2 show the geometry of the initial conceptual design of the transducer. Piezoelectric emitters are located in the central disk and receivers in the external circular crown (Fig. 1). The transducer must be put into physical contact with the tissue (see Fig. 2, bottom part), that will be supposed to be composed of 2 thin layers, dermic and connective.

The oscillation of the emitters generate a circumferential shear movement of the disk, that is transmitted to the tissue and from the latter to the circular crown, that oscillates circumferentially. Finally, this movement is captured by the receivers.

The technique to perform is the time of flight measurement of the signals to extract the shear propagation velocity and from it, the tissular shear modulus.

B. Forward Model

The coupled electrical-mechanic effect of piezoelectricity may be described in the constitutive relations of the dynamic problem assuming linearity, as follows,

$$\mathbf{T} = \mathbf{C}_E \cdot \mathbf{S} + \mathbf{e}^T \cdot \mathbf{E} \qquad (1)$$

$$\mathbf{D} = \mathbf{e} \cdot \mathbf{S} - \varepsilon_{\mathbf{S}} \cdot \mathbf{E} \qquad (2)$$

where ($\mathbf{T}$) is the stress tensor, ($\mathbf{S}$) strain tensor, ($\mathbf{D}$) charge-density displacement, ($\mathbf{E}$) the electric field, $\mathbf{C}_E$ the piezoelectric stiffness matrix, $\mathbf{e}$ the piezoelectric coupling coefficient matrix, $\mathbf{e}^T$ its transposed and $\varepsilon_{\mathbf{S}}$ the permitivity coefficient matrix.

The rest of the problem is given by the equilibrium and cinematic relationships,

$$\nabla \cdot \mathbf{D} = 0; \ \mathbf{E} = -\nabla\phi \qquad (3)$$

$$\nabla^S \cdot \mathbf{T} = 0; \ \mathbf{S} = \frac{1}{2}(\nabla\mathbf{u} + \nabla\mathbf{u}^T) \qquad (4)$$

being $\mathbf{u} = (u_1, u_2, u_3)$ the displacement vector field, and ϕ the electric potential or voltage.

The equations are solved using finite element method implemented in FEAP software, incorporating the boundary conditions. A more detailed description can be found in [6]. Fig. 2 shows the stress distribution on different instants.
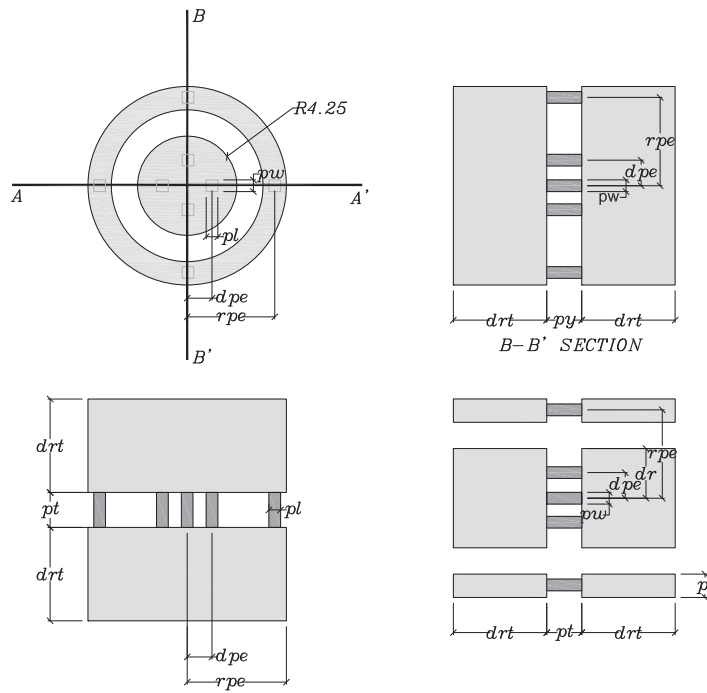
Fig. 1 The geometry of the transducer: Piezoelectric elements are shown in dark gray; four inner elements in the disk are the emitters and four outer elements in the external circular crown are the receivers
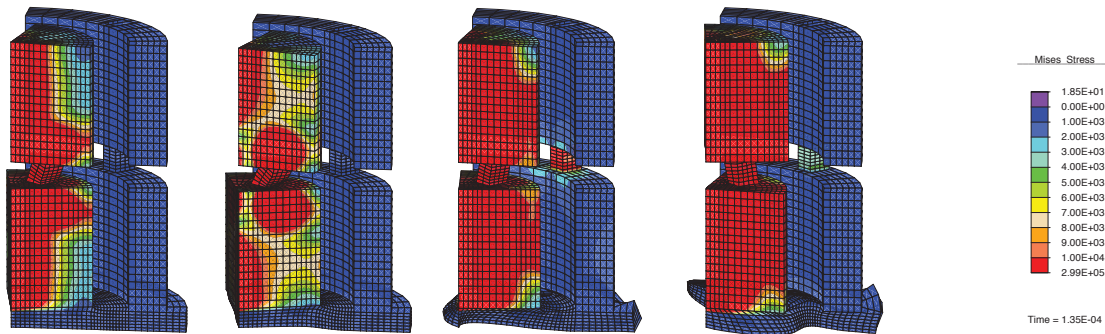

Fig. 2 Torsional transducer at instants $t = 9, 18, 117, 135$ μs: The lower soil is the tissue

C. Probability of Detection

Pathology is inferred when there is a change in the mechanical properties of the tissue layers, in this case, their shear moduli $[G^c \ G^d]$. This means that there are values of reference r for healthy state, and pathology exist if different values are observed $pat_p = [\Delta G^c \ \Delta G^d]$ with $p = c, d$ (the layer, connective and dermic), being $\Delta G^p = G^p - G^p_r$.

The probability of detection (POD) is defined as the probability that the alteration of the received signal caused by the presence of pathology (SIGNAL) exceeds the signal changes originated by noise (NOISE),

$$\text{POD} = P \left(\frac{|\text{SIGNAL}|^2}{|\text{NOISE}|^2} > 1 \right) \quad (5)$$

Consequently, the change in signal and noise must be deduced.

A robust POD (RPOD) is defined, since signal and noise changes are dependent on several parameters pat_p (two in the example $[pat_c \ pat_d]$). RPOD selects the less favourable case,

$$\text{RPOD} = \min_{pat_p} \text{POD}(pat_p) \quad (6)$$

$$\text{POD}(pat_p) = P \left(\frac{|\text{SIGNAL}(pat_p)|^2}{|\text{NOISE}(pat_p)|^2} > 1 \right) \quad (7)$$

The signal variation can be computed applying a Taylor series expansion of the received signal centred at the healthy case and with no noise.

$$\psi_i(pat_p, \sigma) = \psi_i(0,0)$$
$$+ \sum_p \underbrace{pat_p \frac{\mathrm{d}\psi_i}{\mathrm{d}pat_p}(0,0)}_{\text{SIGNAL}(pat_p)} + \underbrace{\sigma \frac{\mathrm{d}\psi_i}{\mathrm{d}\sigma}(0,0)}_{\text{NOISE}} + hot \quad (8)$$

TABLE I
METHODOLOGY

Step	Target	Results	Tools or inputs
1. Forward physical model development	Simulate generation, propagation, and reception of waves	Physical model: differential equations	Conceptual design of the transducer: geometry, materials, etc.
2. Finite element model (FEM)	Computational implementation of the physical model	Computational code of the model	Physical model Boundary cond. (geometry and properties of the conceptual design, etc.)
3. Discretization study	Improve convergence Trade off computational burden-time	Spatial element Time interval	Forward model (FEM) Initial sensor geometry and tissue mechanical properties
4. Validation of FEM results	Assure some accuracy of simulations	Check large discrepancies with approximated models	Use of an analytic simplified torsional (T-wave) model to compare results.
5. Sensitivity analysis on geometric parameters of the transducer	Knowing the response to geometry Select the better materials Minimize P-wave emission Maximize received T-wave amplitude New FEM validation	Knowledge of material influence Better geometric parameters among tested with almost null P-wave and high s/n ratio Ranges of P-wave existence Sensible response, no anomalies	Forward model Established discretization Ranges of geometric parameters Material candidates
6. Sensitivity analysis on mechanical properties $[G^c \quad G^d]$ of tissue	Knowing response in the ranges of G Test P-wave in the whole range of G Forward model validation	No apparent anomalies on response P-wave ranges of existence in tissue	Fordward model Use of selected geometric design, discretization and materials
7. Test of the inverse problem with genetic algorithm (GA)	New test for the forward problem Evaluate convergence of the GA - Quality of identification - Convergence speed	Confirmed right behavior with clear identification of the tissular mechanical properties $[G^c \quad G^d]$ (Fig. 4)	Forward model Misfit cost functional as GA optimization criterion
8. POD evaluation of sensor with better performance in step 5	Evaluate POD of the better design Testing coherency on results	POD graphics on changes of tissue mechanical properties No apparent anomalies	Forward model POD estimator
9. POD optimization	Search the geometric design that maximize RPOD Evaluate difference between better (selected) and best (optimized)	Optimal design Quantification of better-best improvement	RPOD estimator GA with RPOD estimator as GA optimization criterion

being $i = 1, ..., N$ the receiving locations (one in this case). The term labelled SIGNAL represents the variation of the signal originated by pathology, while the term labelled NOISE the variation in the signal originated by noise, from the reference signal $\psi_i(0,0)$ obtained in healthy tissue and no noise.

The derivatives in the SIGNAL can be deduced applying finite differences,

$$
\frac{\mathrm{d}\psi_i}{\mathrm{d}pat_p}(\tilde{pat}_p, 0) = \psi_{i,pat_p}(\tilde{pat}_p, 0)
$$
$$
= \frac{\psi_i(\tilde{pat}_p + \Delta pat_p, 0) - \psi_i(\tilde{pat}_p - \Delta pat_p, 0)}{2\Delta pat_p} \quad (9)
$$

where $\tilde{pat}_p \to 0$ is a very small pathology that guarantees the FEM to capture the perturbations produced at small Δpat_p (since the case $pat_p = 0$ with no pathology needs to be computed with a topologically different mesh). It is important to note that the evaluation of this derivative implies running the FEM code.

The NOISE term needs the following derivative,

$$
\frac{\mathrm{d}\psi_i}{\mathrm{d}\sigma} = \xi_i \mathrm{RMS}(\psi_i^{\mathrm{FEM}}) = \xi_i \mathrm{RMS} \quad (10)
$$

with ξ_i, a random noise generator (a random variable). Applying the expression $|Y_i|^2 = \frac{1}{m}\sum_{i=1}^{m} Y_i^2$ to (5), and introducing (8), (9) and (10),

$$
\mathrm{POD}_p = P\left(\frac{pat_p^2 \frac{1}{N}\sum_{i=1}^{N}(\psi_{i,pat_p}(0,0))^2}{\sigma^2 \mathrm{RMS}^2 \frac{1}{N}\sum_{i=1}^{N}\xi_i^2} > 1 \right) \quad (11)
$$

$$
= P\left(pat_p^2 > \underbrace{\frac{\mathrm{RMS}^2 \sigma^2 \sum_{i=1}^{N}\xi_i^2}{\sum_{i=1}^{N}(\psi_{i,pat_p}(0,0))^2}}_{S_p} \right) \quad (12)
$$

The evaluation of the expressions must be performed running the FEM model, through the functions S_p, that includes the derivative of ψ_i, and RMS. The right hand expression is the probability distribution given by noise translated by the FEM to random variability on the considered parameter (its square). The cumulative probability of this distribution function is,

$$
\mathrm{POD}_p = F\left(\frac{\mathrm{RMS}^2 \sigma^2 \sum_{i=1}^{N}\xi_i^2}{S_p} \right) \quad (13)
$$

Using Monte Carlo techniques and error propagation theory the noise ξ_i in the measurement points can be concluded to follow a normal distribution [12]. In that case, its square ξ_i^2 will be a *Chi-square* distribution, since $\sum_{i=1}^{N}\xi_i^2 \longrightarrow \chi_N^2$ (e.g. [13]). The parameter of the *Chi-square* distribution is the number of degrees of freedom N, which is the number of measurement points. In the case that $N > 10$, the *Chi-square*
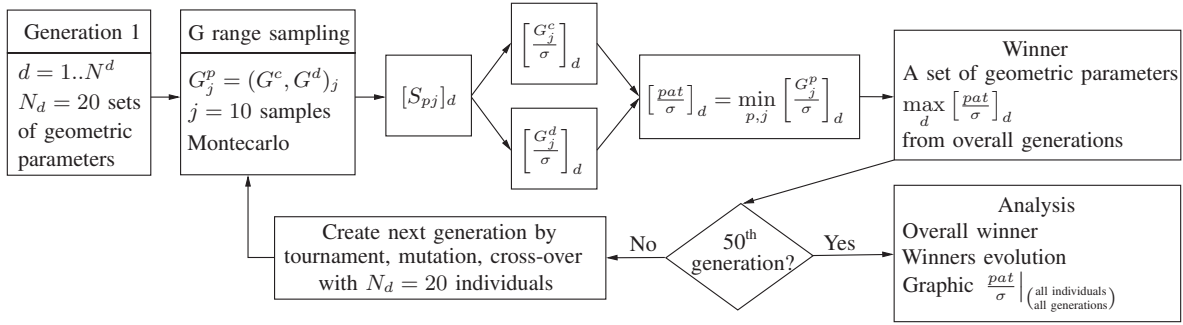
Fig. 3 9th step of methodology: Genetic algorithm to optimize the transducer geometry, maximizing RPOD
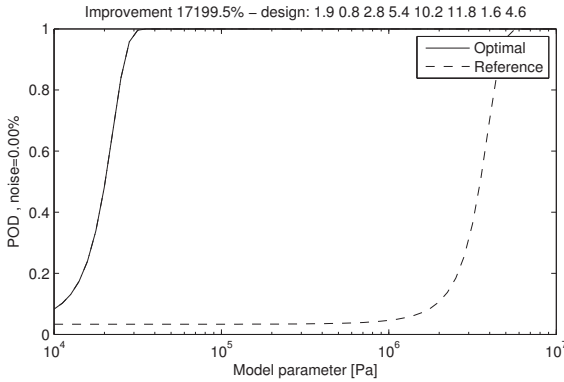

Fig. 4 RPODs of the winner design and the reference design

Fig. 5 Convergence evolution through generations to maximum

distribution can be approximated by a Gaussian or normal N distribution $\chi^2(N) \approx N(N-2/3, \sqrt{2N})$ with mean $N-2/3$ and standard deviation $\sqrt{2N}$. This approximation in (13) yields,

$$pat_p{}^2 \longrightarrow N\left[\frac{\text{RMS}^2\sigma^2(N-2/3)}{S_p}, \frac{\text{RMS}^2\sigma^2\sqrt{2N}}{S_p}\right] \quad (14)$$

Since $F(x) = \int_{-\infty}^{x} f(y)\mathrm{d}y$ is the cumulative of the normal probability density function f, whose inverse is $x = G(F(x))$, the useful pathology severity to noise ratio pat_p/σ can be expressed from (14) given a POD level as,

$$\frac{pat_p}{\sigma} = \sqrt{\frac{\text{RMS}^2(N-2/3)}{S_p}\left(1 + G[\text{POD}_p]\frac{\sqrt{2N}}{N-2/3}\right)} \quad (15)$$

These expressions are only valid for noise with normal distribution at the measurement points. The last one will be further used to optimize the transducer geometry, maximizing the value of the expression. Its evaluation implies running the FEM code to calculate S_p and RMS.

D. Inverse Problem

Inverse problem is used to obtain the optimized parameters of a model that maximize or minimize some condition. Here is used as (1) an additional coherency test on the forward model, looking for tissular mechanical properties that reduce the discrepancy between simulated and experimental signals,
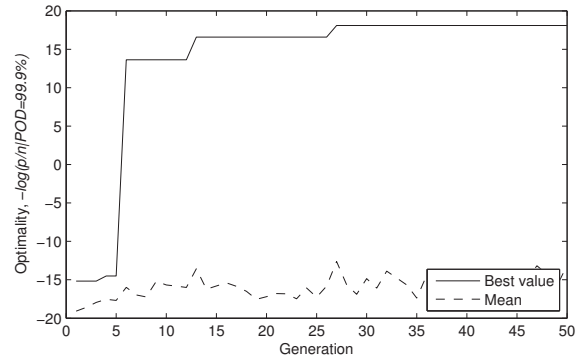
and more importantly (2) to optimize the geometric parameters of the transducer that maximize RPOD.

Genetic Algorithms (GA) are global search algorithms that reasonably explore the whole parameter space to look for the optimal parameters, avoiding the maximization/minimization process to fall in local maxima/minima. More detailed explanation of the algorithm that is used here can be found in [12], [14]. The cost functional is the key point of the optimization criterion. The methodological step 7 uses a misfit function that represents the difference between experimental and simulated signal, to be minimized. More detail can be found in [6]. On the other hand, GA in Step 9 uses 15 as a function to maximize.

If f is the function to optimize, an improved convergence performance of the GA has been reported using an altered version of f [15], consisting of,

$$f^l = \log(f + \epsilon) \quad (16)$$

with ϵ, a very small value that ensure the existence of the logarithm.

E. Methodological Process

Table I, shows the methodological steps that has been followed to develop the models and obtaining the optimal geometry of the transducer that maximizes RPOD. A detailed explanation of steps 1 to 8 can be found in [6].

The optimization process (step 9) is graphically detailed in Fig. 3. It consist of a GA that explores the space of the geometric parameters of the transducer. In this case, it is a
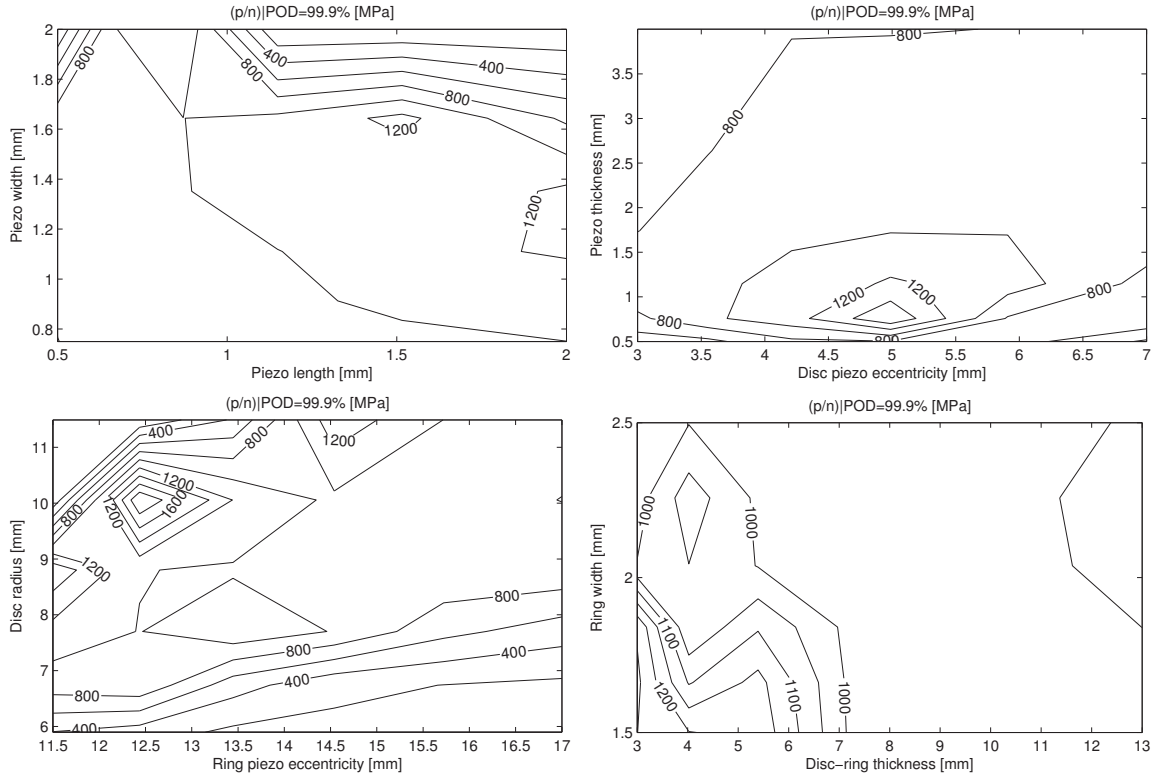
Fig. 6 Slices of the function $\frac{p}{\sigma}$ around the maximum for a 99.9% level of POD

8-dimensional space $[pw, pl, pt, dpe, dr, rpe, rw, drt]$. The GA uses the RPOD as optimization criterion, particularly (15).

A first generation that contains $N_d = 20$ individuals is selected, being each individual a particular sample of the 8D parameter space (a candidate to be the optimal). Each individual d is subject to calculate S_p for a fixed POD level of 99.9%, and a variety of mechanical properties $pat_p = [G^c G^d]$ of the tissue. This sampling of the 2D mechanical parameter space is done using a Montecarlo procedure, obtaining j points $(G^c, G^d)_j$. From these point, a variety of values $S_p j$, with $p = c, d$. The next step is evaluating $[\frac{pat_p}{\sigma}]_j$. The RPOD criteria is applied keeping only the minimum value (the less favorable) of all, disregarding the rest, so that the individual is assigned just one value of $\frac{pat}{\sigma}$ from all calculated. Comparing the results of the $N_d = 20$ individuals, the winner of the generation will be the one with higher value of $\frac{pat}{\sigma}$ (maximum RPOD). A new generation is created from the current one with new $N_d = 20$ individuals, applying operations of mutation, tournament and crossover [14]. After dealing with this second generation its winner is compared with the former, keeping the best of both. This process is repeated for 50 generations.

III. RESULTS

The results of the optimization are, (1) a winner individual, in terms of the best geometric properties of the transducer that maximize RPOD, (2) the discretely sampled 8-dimensional function $\frac{pat}{\sigma}(pw, pl, pt, dpe, dr, rpe, rw, drt)$ of all individuals tested from all generations, to check the quality of the maximum, and finally (3) the convergence evolution of the successive winners towards the maximum.

Table II shows the winner geometric parameters of the transducer (Opti. column), and the reference values were used in the methodological steps previous to optimization with POD maximization (Ref. column).

TABLE II
DIMENSIONS OF TRANSDUCER: CONSIDERED RANGES OF VARIATION, REFERENCE VALUES AND POD OPTIMIZED VALUES

Design Parameters [mm]	Range	Ref.	Opti.	Label
Piezoelectric Width	[0.75 2]	1	1.9	pw
Piezoelectric Length	[0.5 2]	1	0.8	pl
Piezoelectric Thickness	[0.4 4]	2	2.8	pt
Disc Piezoelectric Eccentricity	[1.5 3.5]	2.5	2.7	dpe
Disc Radius	[1.75 5.75]	4.25	5.1	dr
Ring Piezoelectric Eccentricity	[5.75 8.5]	7.5	5.9	rpe
Ring Width	[1.5 2.5]	2	1.6	rw
Disc-Ring Thickness	[3 13]	8	4.6	drt

Fig. 4 presents the RPOD curve of two transducer designs, the winner and the reference. The winner shows a higher sensibility to detect lower changes in the mechanical properties for the same values of POD. This represents a 17,199.5% of improvement (about 172 times). The evolution of the convergence trough the generations can be observed in Fig. 5, where the winner has been captured by about 27th generation.

The GA implies a sampling of the function $\frac{pat}{\sigma}$ in the 8-dimensional space of geometric parameters. Fig. 6 shows different slices of the function around the maximum.

The final geometry of the transducer leads to a central frequency of 28kHz.

IV. CONCLUSION

A method to optimize the geometry of a torsional transducer has been shown. The optimization is aimed to maximize the probability of detection in a two-layer tissue. The use of torsional waves is based on the evidences of their higher sensitivity to changes in the tissular microstructure, correlated with shear modulus changes. A genetic algorithm has been developed in order to implement the optimization process, with a cost functional derived from the POD. The geometric parameter space is globally sampled through several generations and another sampling of the tissular mechanical properties is performed on each generation. The POD is always calculated selecting the less favorable case, constituting a robust POD criterion.

An iterative sequence of prototypes are being produced to test the real performance of the transducer, and to solve new non-simulated problems related to radioelectrical and mechanical isolation, alignments and transducer calibration.

ACKNOWLEDGMENT

REFERENCES

[1] S. Van Kervel and J. Thijssen, "A calculation scheme for the optimum design of ultrasonic transducers," *Ultrasonics*, vol. 21, no. 3, pp. 134–140, 1983.
[2] D. Bader and P. Bowker, "Mechanical characteristics of skin and underlying tissues in vivo," *Biomaterials*, vol. 4, no. 4, pp. 305–308, 1983.
[3] A. S. Ahuja, "Tissue as a voigt body for propagation of ultrasound," *Ultrasonic Imaging*, vol. 1, no. 2, pp. 136–143, 1979.
[4] J. Pereira, J. Mansour, and B. Davis, "Dynamic measurement of the viscoelastic properties of skin," *Journal of Biomechanics*, vol. 24, no. 2, pp. 157–162, 1991.
[5] T. Bigelow, B. McFarlin, W. O'Brien Jr., and M. Oelze, "In vivo ultrasonic attenuation slope estimates for detecting cervical ripening in rats: Preliminary results," *Journal of the Acoustical Society of America*, vol. 123, no. 3, pp. 1794–1800, 2008, cited By (since 1996) 0.
[6] J. Melchor and G. Rus, "Torsional ultrsonic transducer computational design optimization," *Ultrasonics*, vol. 50, no. 7, pp. 1950–1962, 2014.
[7] B. L. McFarlin, W. D. O'brien, Jr., M. L. Oelze, J. F. Zachary, and R. White-Traut, "Ultrasound insertion loss of the rat cervix," *American Journal of Obstetrics and Gynecology*, vol. 193, no. 6, Supplement 1, pp. S154–S154, 2005, 26th Annual Meeting of the Society for Maternal-Fetal Medicine - The Pregnancy Meeting.
[8] B. L. McFarlin, W. D. O'Brien, M. L. Oelze, J. F. Zachary, and R. C. White-Traut, "Quantitative ultrasound assessment of the rat cervix," *Journal of ultrasound in medicine*, vol. 25, no. 8, pp. 1031–1040, 2006.
[9] M. Lebertre, F. Ossant, L. Vaillant, S. Diridollou, and F. Patat, "Spatial variation of acoustic parameters in human skin: an in vitro study between 22 and 45 mhz," *Ultrasound in medicine & biology*, vol. 28, no. 5, pp. 599–615, 2002.
[10] F. Sebag, J. Vaillant-Lombard, J. Berbis, V. Griset, J. Henry, P. Petit, and C. Oliver, "Shear wave elastography: a new ultrasound imaging mode for the differential diagnosis of benign and malignant thyroid nodules," *Journal of Clinical Endocrinology & Metabolism*, vol. 95, no. 12, pp. 5281–5288, 2010.
[11] J. M. Chang, W. K. Moon, N. Cho, A. Yi, H. R. Koo, W. Han, D.-Y. Noh, H.-G. Moon, and S. J. Kim, "Clinical application of shear wave elastography (swe) in the diagnosis of benign and malignant breast diseases," *Breast cancer research and treatment*, vol. 129, no. 1, pp. 89–97, 2011.
[12] G. Rus, S. Y. Lee, S. Y. Chang, and S. C. Wooh, "Optimized damage detection of steel plates from noisy impact test," *International Journal for Numerical Methods in Engineering*, vol. 68, pp. 707–727, 2006.
[13] L. Rade and B. Westergren, *Mathematics Handbook for Science and Engineering*. Springer, 1999.
[14] D. Goldberg, *Genetic algorithms in search, optimization and machine learning*. Addison-Wesley Publ, Reading, Massachussets, etc., 1989.
[15] R. Gallego and G. Rus, "Identification of cracks and cavities using the topological sensitivity boundary integral equation," *Computational Mechanics*, vol. 33, pp. 154–163, 2004.